Probing Surface-Mediated Electronic Coupling in Flat Hexagonal Phosphorus Nanostructures and Monolayer on Au(111)

Abhishek Karn, Ian-evan Michel, Mahé Lezoualc'H, Cyril Chacon, Yann Girard, Alexander Smogunov, Yannick Dappe, J. Lagoute

▶ **To cite this version:**

Abhishek Karn, Ian-evan Michel, Mahé Lezoualc'H, Cyril Chacon, Yann Girard, et al.. Probing Surface-Mediated Electronic Coupling in Flat Hexagonal Phosphorus Nanostructures and Monolayer on Au(111). Small, 2024, pp.2405924. 10.1002/smll.202405924 . hal-04760585

HAL Id: hal-04760585
https://hal.science/hal-04760585v1

Submitted on 30 Oct 2024

HAL is a multi-disciplinary open access archive for the deposit and dissemination of scientific research documents, whether they are published or not. The documents may come from teaching and research institutions in France or abroad, or from public or private research centers.

L'archive ouverte pluridisciplinaire **HAL**, est destinée au dépôt et à la diffusion de documents scientifiques de niveau recherche, publiés ou non, émanant des établissements d'enseignement et de recherche français ou étrangers, des laboratoires publics ou privés.

Distributed under a Creative Commons Attribution - NonCommercial - NoDerivatives 4.0 International License

Probing Surface-Mediated Electronic Coupling in Flat Hexagonal Phosphorus Nanostructures and Monolayer on Au(111)

A. Karn I.-E. Michel M. Lezoualc'h C. Chacon Y. Girard A. Smogunov Y. J. Dappe J. Lagoute

Dr. A. Karn, Dr. C. Chacon, Dr. Y. Girard, Dr. J. Lagoute
Laboratoire Matériaux et Phénomènes Quantiques, CNRS-Université Paris Cité, 10 rue Alice Domon et Léonie Duquet, 75205 Paris Cedex 13, France.
jerome.lagoute@u-paris.fr
I.-E. Michel, M. Lezoualc'h, Dr. A. Smogunov, Dr. Y. J. Dappe
SPEC, CEA, CNRS, Université Paris-Saclay, CEA Saclay, 91191 Gif-sur-Yvette Cedex, France

Keywords: *Phosphorene, Scanning Tunneling Microscopy, Density Functional Theory*

Due to its diverse allotropes and intriguing properties, two-dimensional (2D) phosphorus, also known as phosphorene, is a material of great interest. Here, we report on the successful growth of flat hexagonal 2D phosphorus on Au(111). Starting from phosphorus linear chains at low coverage, we formed a porous network and finally an extended 2D flat hexagonal (HexP) layer while increasing phosphorus deposition. Using scanning tunneling microscopy/spectroscopy combined with *ab initio* calculations, we follow the structure and electronic properties of the as grown phosphorus structures. We observe the progressive formation of a phosphorus electronic band in the conduction band region. More strikingly, we observe a partial flatband that appears only on the HexP phase characterized by a sharp peak in the electronic spectrum. These bands arise from the hybridization of phosphorus and gold atoms. This novel phosphorus based structure exhibits remarkable electronic properties due to gold mediated phosphorus-phosphorus electronic coupling. This work paves the way for new interface material developments with attractive electronic properties.

1 Introduction

The quest for novel two dimensional (2D) materials with exotic electronic properties holds great promises for next generation electronics [1, 2]. Among these, phosphorene, a single layer of phosphorus atoms, and its bulk counterpart, black phosphorus (BP), have garnered significant interest due to their exceptional characteristics [3, 4, 5]. These include high carrier mobility, tunable bandgap, optical, thermal and mechanical properties [6, 7, 8, 9]. Unlike graphene, a single flat layer of sp^2-hybridized carbon atoms, phosphorene exhibits a unique non-planar puckered structure of sp^3-hybridized phosphorus atoms [7, 8]. This structure offers an additional degree of freedom through the rotation around P-P bonds, that has led to the prediction of a vast number of potential phosphorus allotropes [10, 11, 9], all exhibiting non-planar structures. The tunability of phosphorene bandgap and the variety of its possible structural phases constitute the main advantages of phosphorene as compared to other 2D materials. The experimental realization 2D phosphorus remains in its early stage [12], however a few synthesis methods have been successful. Among them, the honeycomb structure blue phosphorene (BlueP) has received extensive attention. Initially proposed theoretically [13], it was subsequently synthesized via *in situ* growth on Au(111) [14], exhibiting a bandgap of 1.1 V. Later, the epitaxial growth of phosphorene has been carried out on different substrates such as Cu(111), tellurium functionalized Au(111) [15] or silicon intercalated Au(111) [16], resulting in the formation of nanoclusters, single phosphorus atoms, honeycomb BlueP and (1×1) BlueP, depending on the strength of coupling at the phosphorus-substrate interface. Honeycomb BlueP has also proved to exhibit a Dirac cone, similarly to graphene, due to an important interfacial stretch which makes it planar [17].Indeed, the interaction of 2D materials with supporting substrate is a crucial factor influencing their properties [18]. In particular, the formation and control of interfacial electronic states is essential for tailoring the electronic properties of 2D materials for specific innovative applications.

Here we report the fabrication of non-conventional 2D phosphorus allotrope. In contrast to the mostly reported non-planar 2D phosphorus structures, we synthesized a hexagonal packed flat phosphorus monolayer on Au(111) surface. We used scanning tunneling microsopy (STM) and spectroscopy (STS) to systematically study the growth, atomic structure and electronic evolution of the flat phosphorus layer when increasing the coverage. The differential conductance (dI/dV) measurement shows a remarkable evolu-

tion of the electronic states in the conduction band. Our *ab initio* calculations reveal the band structure and the origin of the experimentally observed electronic features that arise from P-Au hybridization.

2 Results and discussion

Figure 1a presents the early stage of phosphorus growth on Au(111). Phosphorus deposition at room temperature followed by annealing at 185 °C (details in methods) leads to the formation of linear phosphorus nanostructures. Higher resolution imaging (Fig. 1b) reveals that the linear nanostructures consist in double (rarely single) atomic rows. These nanochains exhibit characteristic branched features at 120 ° angles and can incorporate single or multiple rings. Interestingly, the Au(111) reconstruction is significantly altered by the phosphorus deposition. Discommensuration lines transform into trigon shapes surrounding the nanostructures. The modification of the herringbone reconstruction may arise from a relaxation of the Au(111) surface induced by the interaction with the phosphorus atoms. Note also that the incorporation of phosphorus in Au(111) can result in the modification of the surface reconstruction [16]. The observation of double atomic chains nanostructures is different from previous studies reporting on P chains on Au(111) [16, 19] where the linear structures where made of single atomic rows and no reorganization of discomensuration lines was observed. This discrepancy may be due to difference in the growth procedure (no post-annealing [16], or growth on a heated Au(111) substrate [19]). Single P atom chains where also discussed theoretically and identified as resulting from a competition between the interaction among P atoms and the attraction on P atoms by Au substrate [20].

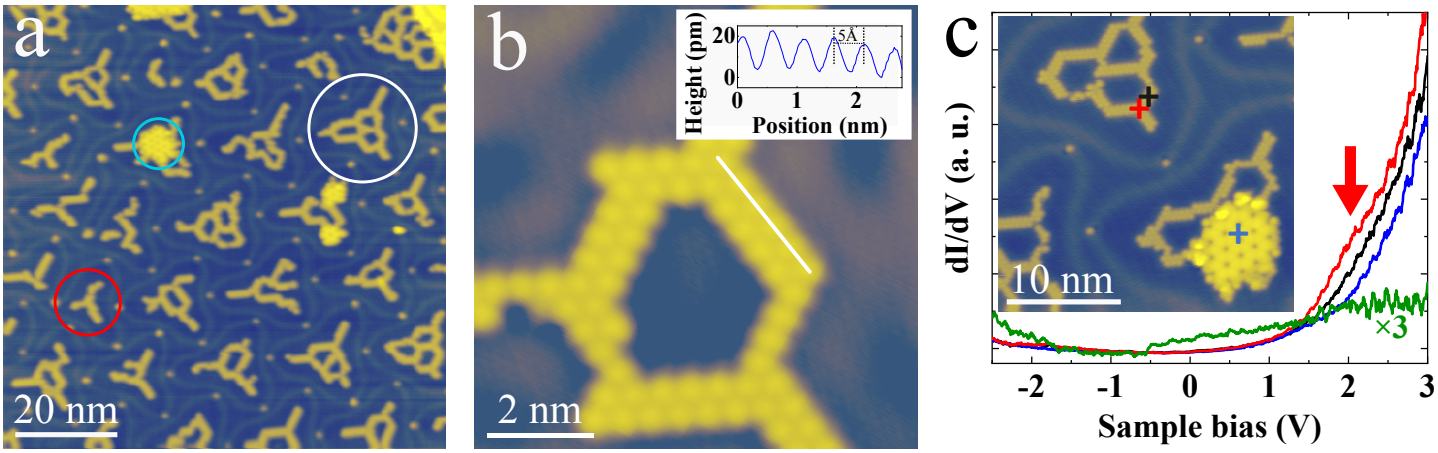

Figure 1: (a) Large scale STM topography of phosphorus nanostructures ($V = 1$ V, $I = 10$ pA). Three directional chains, multiple rings, and BlueP are highlighted by red, white, and cyan color circles respectively. (b) Atomic resolution image of phosphorus ring taken on another Au(111) single crystal ($V = 0.05$ V, $I = 10$ pA). The lattice spacing of P chains or rings nanostructure is 5 Å, as shown by the white line profile in the inset. (c) LDOS spectrum of phosphorus nanostructures. Inset image ($V = 1$ V, $I = 50$ pA) shows the tip positions of acquired LDOS spectrum respectively. The color of the cross corresponds to the respective color spectrum. For better visibility of Au(111) Shockley state, the corresponding spectrum is three times enhanced.

Interestingly, Blue phosphorene (BlueP) islands can be seen on our sample with characteristic hexagonaly arranged triangular structures. This is indicative that under our growth conditions, the BlueP and nanostructure phases are coexisting. In the nanostructures, each bright dot corresponds to a single phosphorus atom, as confirmed by the disruption of these nanostructures under voltage pulses applied with the STM tip (see Supplementary Information Fig. S1). The distance between neighbouring atoms in these structures is 5 Å, significantly larger than that of bulk BP or BlueP *i.e.* 2.2 Å. This corresponds to a $\sqrt{3} \times \sqrt{3}R30°$ superstructure with respect to the Au(111) atomic lattice parameter (2.88 Å). This large interatomic distance prevents from direct electronic coupling between P atoms. However, as we will show below, an indirect coupling involving hybridization with the Au(111) substrate leads to the formation of new electronic bands.

We have investigated the electronic properties of these nanostructures by dI/dV spectroscopy (Fig. 1c). The tip calibration was verified by measuring the Au(111) spectrum, which showed the expected onset of the Shockley surface state around -0.5 V. Interestingly, the BlueP exhibited a featureless spectrum [21], and the P chains themselves lacked remarkable features within the probed energy range. However, a small bump appeared around 2 V at the junction areas where two chains meet within a ring. As will be discussed below, this feature will become more prominent in larger structures.

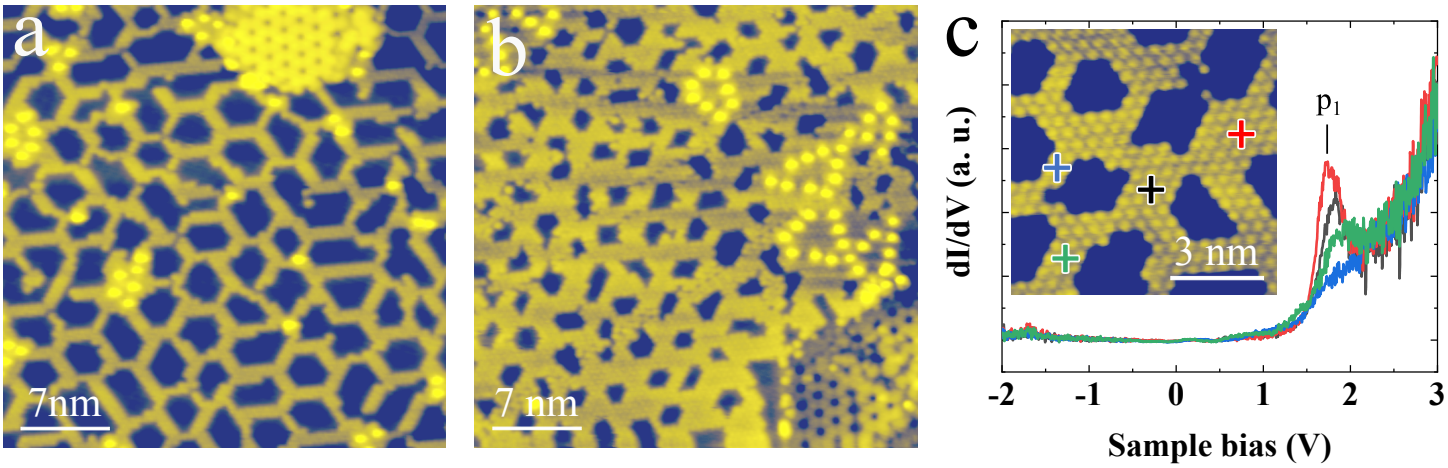

Figure 2: Topography of phosphorus porous network after deposition time of (a) 10 minutes and (b) 20 minutes respectively ($V = 1$ V, $I = 50$ pA). (c) LDOS spectrum of phosphorus porous network. Inset image ($V = 0.5$ V, $I = 50$ pA) shows the tip position of acquired LDOS spectrum. The color of the cross corresponds to the respective color spectrum.

Following the characterization of the initial growth stage, we investigated the evolution of the system under increased P coverage. Figure 2a,b depicts the surface morphology after a total deposition time of 10 and 20 minutes respectively. In both cases, the Au(111) substrate is predominantly covered with interconnected chains forming a porous network on the surface. These chains exhibit a diatomic thickness in low coverage samples, similar to double lines in nanostructures. At higher coverages, the chain width increases to 6-7 atomic size, with the atoms arranged in a hexagonal pattern and a consistent 5 Å lattice spacing. STS was then used to probe the electronic properties of this network. Figure 2c shows the dI/dV spectra for the high coverage network (see Fig. S2 for low coverage data). In both cases, the dI/dV spectra reveal a strong dependence of the shoulder feature near 2V in the LDOS on the atomic chain width. Notably, the shoulder in 2-3 atomic thick chains transforms progressively into a distinct peak (P1) at 1.75 V in 6-7 atomic thick chains. These observations suggest the gradual formation of an electronic band within the hexagonal P structures as their size increases. To explore this further, we proceeded with additional deposition aiming for a complete monolayer.

In Fig. 3a, we show a hexagonal phosphorus (HexP) monolayer obtained after a deposition time of 27 minutes. Unlike other phosphorus phases like BP or BlueP, which exhibit puckered structures, HexP is atomically flat. The interatomic distance within the HexP monolayer (5 Å) is identical to that observed in the above-mentioned nanostructures. Atomic-resolution imaging reveals a 30° rotation of the HexP lattice relative to the Au(111) substrate, corresponding to a $\sqrt{3} \times \sqrt{3}R30°$ HexP structure. Such structure has also been obtained by thermal decomposition of InP on Au(111) [19], but the electronic properties were not investigated. We performed spectroscopy measurements on HexP monolayer in order to investigate the electronic properties (Fig. 3b). Similarly to the porous network, a broad peak is observed at 1.75 V (P1). Intriguingly, a sharp new peak appears at 1.6 V (P2), which is unprecedented for phosphorus monolayers. This sharp peak is consistently observed only on the HexP monolayer and not on the chain or porous phosphorus structures obtained at lower coverages. This suggests that an extended HexP structure is crucial for the emergence of this peak. This is further confirmed by the spectral evolution near a Au(111) step edge. Figure 3c) shows a monolayer phosphorus across a Au(111) step edge. At the step edge, the spectrum resembles that of a 3-4 atom thick chain, exhibiting a shoulder near 2

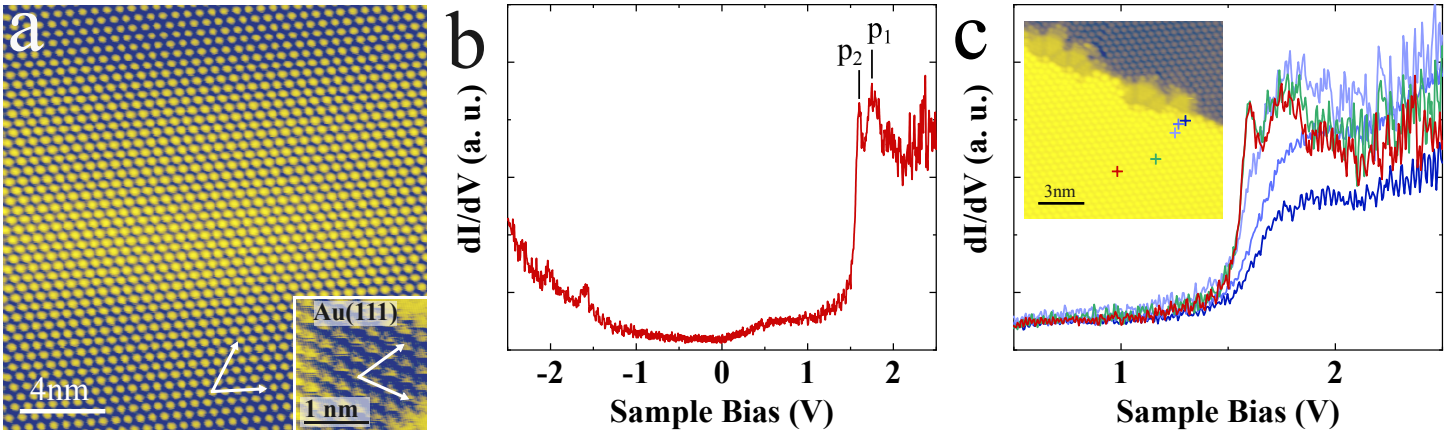

Figure 3: (a) Atomic resolution topography of HexP monolayer ($V = 1$ V, $I = 50$ pA). The inset shows the Au(111) lattice. The white arrows indicate two in-plane lattice directions. (b) LDOS spectrum of HexP monolayer. The two peaks P1 and P2 are at 1.75 V and 1.6 V. (c) The spatial evolution of LDOS in HexP monolayer. The tip positions are highlighted with a cross in the inset image ($V = 1$ V, $I = 50$ pA). The color of the cross corresponds to the respective color spectrum.

V. As we move away from the edge, the shoulder transforms into P1 peak , characteristic of a 6-7 atom thick chain. Notably, the P2 peak only appears when the tip is positioned sufficiently far from the edge. This spatial dependence of the sharp and broad peaks around the step edge is corroborated by the conductance (dI/dV) mapping (Supplementary Information, Fig. S3). The intensity of the 1.75 V state increases near the step edge, while the intensity of the 1.6 V state decreases.

To gain a deeper insight into these electronic features, we have performed Density Functional Theory (DFT) calculations of the electronic structure of HexP on Au(111). The corresponding unit cell, consisting in one P atom on a slab of 15 Au atomic layers is shown in Fig. 4a). The choice of 15 Au layers is motivated by the suppression of the interaction between the top and bottom gold surfaces, so as to avoid a splitting between the corresponding surface states. The full band structure in Fig. 4b reveals as expected a similar electronic behavior compared to pristine Au(111), with a quasicontinuum of states (yellow) and a defined pseudogap region containing 6 electronic bands crossing the Γ point. The prominent free-electron-like band at -0.55 eV corresponds to the well-known bare Au(111) surface state (bottom surface) as confirmed by the projected band structure of Fig. 4e. The W-shaped band just above the parabolic band is the new surface state (top surface) - modified by the presence of the HexP-monolayer (Fig. 4f). To elucidate the charge transfer processes, we computed the evolution [22] of the total and the projected band structures as the HexP-monolayer is brought down from 5 Å above its final position to its relaxed state (animation in Supporting Information and ref. [22]). During this process, notably the P-derived surface state remain parabolic and is progressively shifting downwards. As the HexP-monolayer approaches its equilibrium position and interacts more strongly with the Au surface, the modified surface state folds back upwards locally around the Γ point, transferring electrons to the HexP-monolayer, resulting in its characteristic W-shape. It's worth noting that the $\sqrt{3} \times \sqrt{3}$ pattern of the adsorbed P layer induces a slight structural modification of the Au surface. To isolate the effect of the P layer from the surface modification, we calculated the band structure with the P atoms removed but the Au surface structure preserved (Fig. S4). The absence of the significant upward shift observed with P confirms that the shift arises from charge transfer between Au and P.

A particularly striking feature of the band structure in Fig. 4b is a flat part around the Γ point at 2.42 eV above the Fermi level (see Fig. 4d for a zoom-in). This unusual feature could potentially influence material properties. The analysis of the projected band structure indicates that this flatband arises from the hybridization of the s and p_z orbitals of P atoms and of the s orbital of Au atoms (Fig. 4f-h). In other words, this analysis indicates that the flatband is a direct consequence of the coupling between the phosphorus layer and the Au substrate.

Based on the calculated band structure and density of state (DOS), the STM spectroscopy measurements can be interpreted as follows. The total DOS calculated for the HexP-monolayer exhibits signifi-

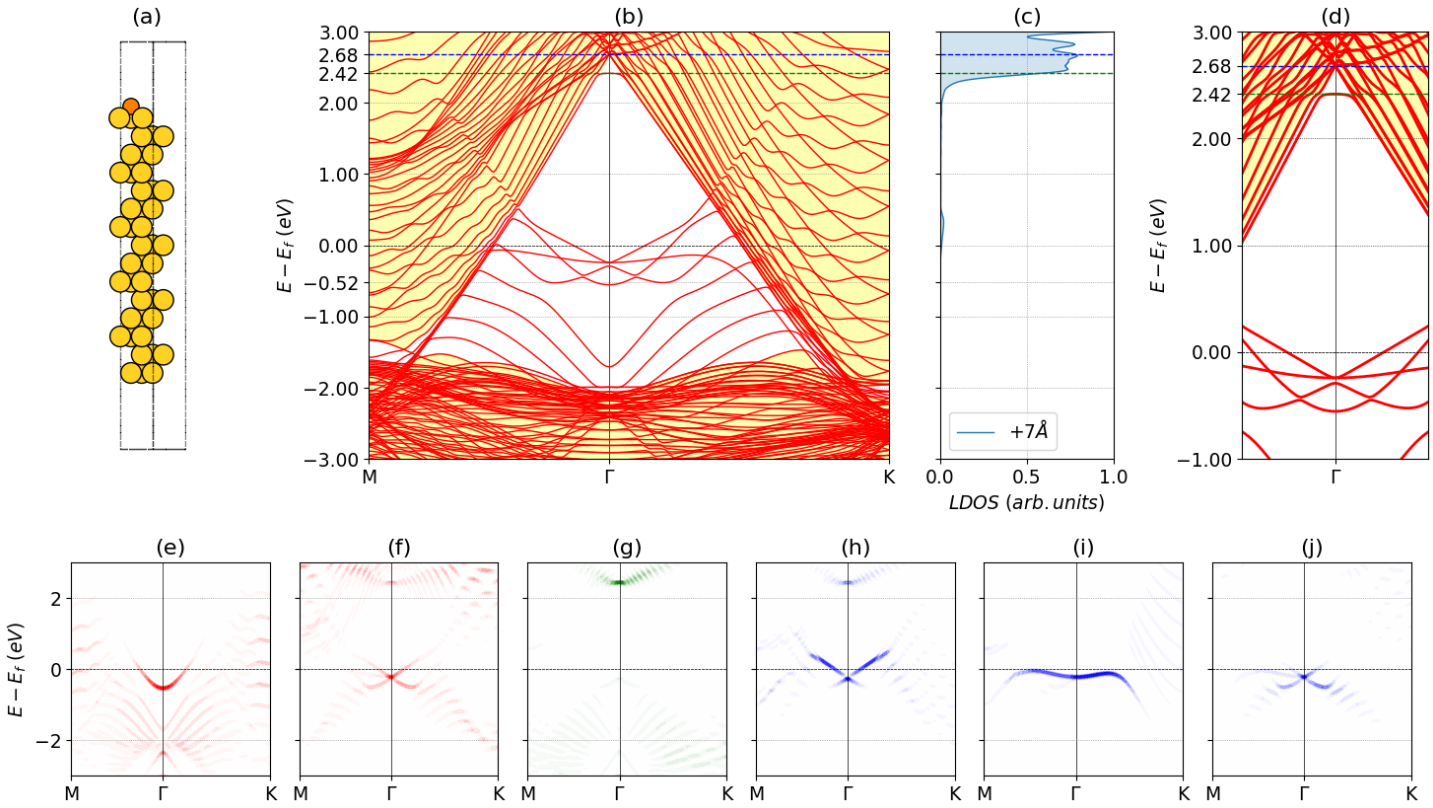

Figure 4: (a) Unit-cell of HexP phosphorus monolayer on Au(111) (b) Band structure of HexP phosphorus monolayer on Au(111) with the quasi-continuum of states in yellow (c) LDOS calculated 7$\AA$ above the P atoms filtered in k-space to one half of the Brillouin zone (d) Zoom around the Γ point of the band structure (e) Band structure projected on p_z orbitals of the bare Au(111) surface, (f) on s orbitals of the P-modified Au(111) surface, (g) on phosphorus s orbital, (h) on phosphorus p_z orbital, (i) on phosphorus p_x orbital, (j) on phosphorus p_y orbital.

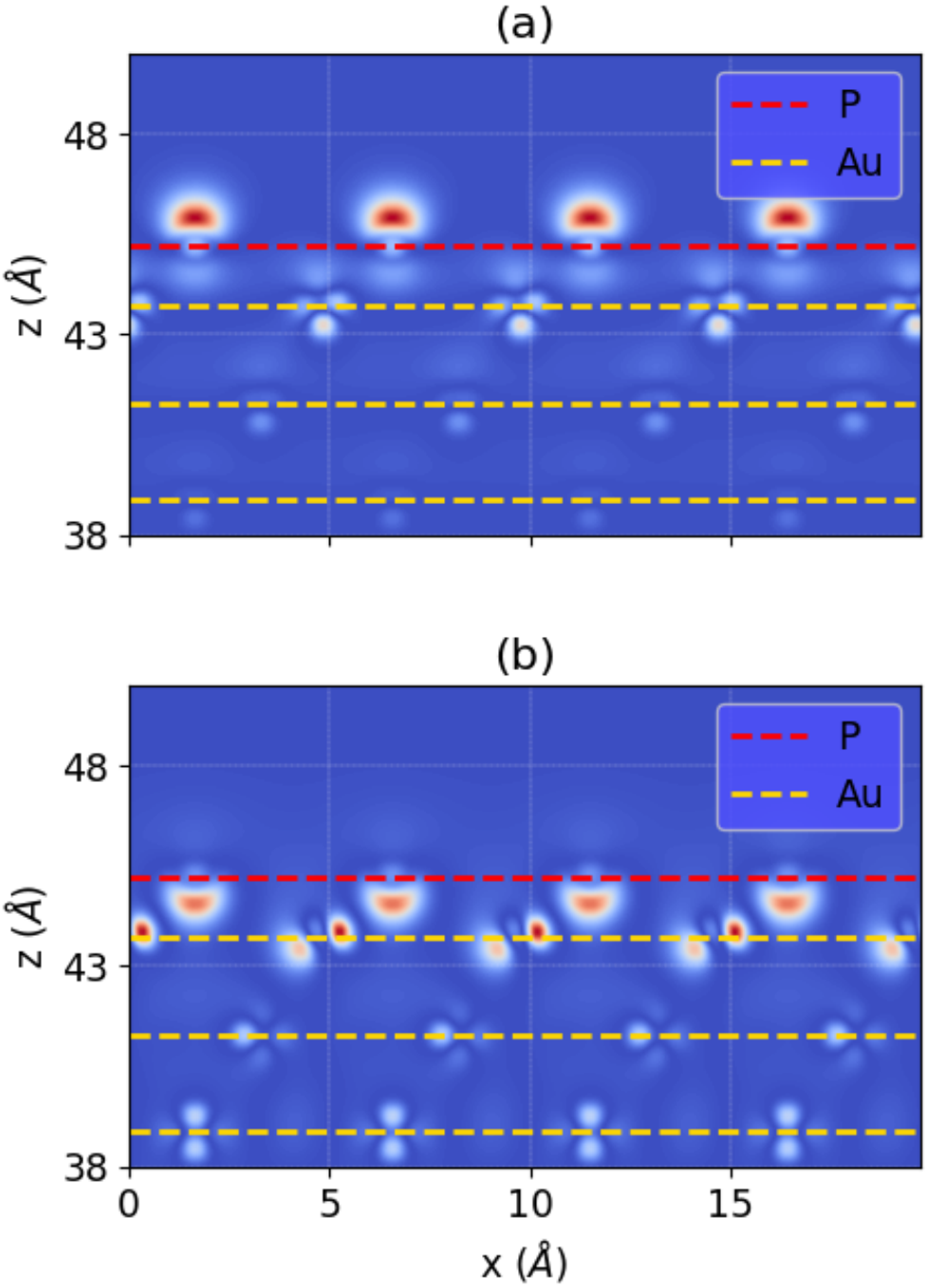

Figure 5: (a) 2D charge density cut of the new surface state (W-shaped band) with minimum at −0.52 eV (b) 2D charge density cut of the flat band at 2.42 eV

cant contributions from both occupied and unoccupied states near the Fermi level (Fig. S5a), it deviates from the experimental STM spectrum dominated by unoccupied high-energy states. Such deviation is not surprising since the dI/dV signal in STS measurements is related to the LDOS. Moreover, the STS is dominated by the states close to the Γ point. Our calculations of the vacuum LDOS within a cubic box at varying heights (Fig. S5b) reveal a dominance by the conduction band states around 2 eV due to their larger spatial extension into the vacuum. The LDOS calculated for a specific height (7 Å above P atoms) and filtered to one half of the Brillouin zone is shown in Fig. 4c. It exhibits excellent agreement with the experimental data. The calculated LDOS is dominated by empty states and reproduces the p_2 and p_1 features observed. The p_2 peak originates from the flatband, while the p_1 peak comes from a series of electronic bands. Band structure projections reveal that both peaks arise from the coupling of s and pz orbitals of P and s orbital of Au.
To deepen our understanding, we have calculated the spatial distribution of the charge density corresponding to the electronic band involved in the flatband (Fig. 5b). The calculations confirm that the state corresponding to the flatband is localized at the interface between the phosphorus layer and the Au substrate, which is consistent with the identified orbital contributions. Additionally, the calculations show that the shifted surface state is centered on the P layer and extends into the vacuum region (Fig. 5a). Therefore, the electronic structure of the HexP layer on Au(111) can be understood as a result of the interaction between P atomic orbitals and the Au(111) surface state, leading to an upshifted surface state and an unoccupied flatband. Moreover, this phosphorus-induced flat band represents also a signature that despite their rather large interatomic distance (5 Å), preventing direct coupling between the phosphorus atoms, these atoms are coupled indirectly through the gold substrate. As a result, we have observed here a new kind of atom/metal interface where the atoms interact through a surface-mediated electronic coupling and whose electronic properties depend on the specific chemical affinity between the adsorbate atoms and the metallic substrate. Note that the control of phosphorus amount deposited on the surface allows to reach different structures (chains, porous network, periodic lattice), which can be exploited to design phosphorus based applications.

3 Conclusion

In summary, we used on-surface synthesis to realize hexagonal flat phosphorus nanostructures and monolayer on Au(111). When increasing the phosphorus coverage, linear chains, porous network and ultimately phosphorus hexagonal monolayer (HexP) are obtained. The LDOS shows the progressive formation of an unoccupied broad peak when the size of the phosphorus nanostructures increases. For the monolayer HexP phase, a sharp peak appears below this broad peak. DFT calculations elucidate the origin of the flat HexP electronic structure. The hybridization between phosphorus atoms and the Au(111) substrate plays a crucial role, not only modifying the Au(111) surface state but also leading to the formation of a flat band arising from the hybridization of P and Au orbitals. As a consequence, this new 2D phase of phosphorus also exhibits a particular interface behavior with gold, as phosphorus atoms are indirectly coupled through the gold substrate leading to the observed flat band. Note that the position of the flat band is related to the chemical affinity of the two interacting materials and the corresponding charge transfer between gold and phosphorus. Another material combination might lead to a different charge transfer and a resulting flat band much closer to the Fermi level. Hence, this work paves a new way for exploring sparse atomic structures deposited on surface, with desirable exotic electronic properties.

4 Methods

4.1 Sample Growth and Characterization

The sample growth was performed in a preparation chamber maintained at 2.10^{-10} mBar. phosphorus flux was directed on Au (111) substrate at room temperature, by evaporating black phosphorus crystals at 230 °C in a K-Cell from MBE-Komponenten. The samples were then transferred to the UHV anal-

ysis chamber without air exposure. The supplementary Fig. S6 shows the deposition of phosphorus on Au(111) at room temperature and without post-growth treatment. After deposition, the samples were annealed at 185 °C for 2 hours. We repeated the growth on various single crystal samples to verify the yield of the phosphorus nanostructures (Figs. S7, S8). All the STM/STS measurements were performed at low temperatures on a Scienta-Omicron Fermi DryCoolTM STM. The instrument employs a Gilford-McMahon refrigerator and a cold finger for reaching approximately 8 K on the STM head. An exchange gas reservoir is used to transfer the cooling power to the STM head avoiding any mechanical coupling with the UHV Chamber.

4.2 Computational details

The *Ab initio* calculations have all been performed using the Quantum ESPRESSO [23, 24] suite of plane-wave based DFT codes. All calculations and data produced for the study of the HexP layer on Au(111) have been done and tracked using AiiDA [25, 26, 27] (Automated Interactive Infrastructure and Database for Computational Science), an open-source Python infrastructure which allows to track data provenance. The AiiDA database containing the whole relaxation procedure, the SCF calculation and all post-processing results such as DOS, PDOS, LDOS, filtered-LDOS, band structure and charge densities is linked in the references [28].
To model the Au(111) surface, a slab of 15 gold layers is used. This choice ensures that the gold surface states interact minimally with each other, approaching the conditions of a semi-infinite surface. It also prevents a significant lifting of degeneracy of the two surface states, which would ultimately affect adsorption properties. Also, since the Au(111) surface is 3-layer periodic, it is important to have a slab with a number of layers that is a multiple of this periodicity for good convergence of surface properties (see reference [29]). An irreducible unit-cell (or IUC) with a filament of 15 gold atoms and 10 Å of vacuum on each side is used to model the gold slab, ensuring that there is no interaction between the periodically repeated slabs and enough space to perform LDOS calculations. After doing a cell volume relaxation and a relaxation of the top 3 gold atoms where the phosphorus layer will be added, the unit-cell (or UC) lattice vectors are those of an HEX($a = 2.85$ $\mathring{A}, c = 53.76$ $\mathring{A}$) Bravais lattice.
Calculated band structures of the bare Au(111) slab of 15 layers with LDA, PBE and PBEsol exchange-correlation functionals show that the PBEsol gives the most accurate Au(111) surface state energy, i.e. -0.5 eV. LDA and PBE give respectively -0.7 eV and -0.3 eV for the surface state energy. Based on these results all following computations have been done using the PBEsol functional [30]. Pseudopotentials are retrieved from the *SSSP Efficiency (v1.3.0)* library maintained by MaterialsCloud. This functional gives also a good atomic lattice parameter of Au(111) of 2.85 Å instead of the experimental 2.88 Å.
To model the experimental structure of an HexP layer on a Au(111) surface, we used a $\sqrt{3} \times \sqrt{3}$ $R30°$ "super-cell" of the previous IUC with 3 filaments of 15 gold atoms and a direct basis. Cell lengths and angles are then the following : $a_1 = a_2 = 4.92878$ $\mathring{A}$, $a_3 = 53.764$ $\mathring{A}$, $\alpha_1 = \alpha_2 = 90°$ and $\alpha_3 = 60°$. A phosphorus atom is then added at 1.423 $\mathring{A}$ above an fcc site on top of the Au(111) slab to form the unit cell of the full periodic structure. The fcc site is indeed the one showing the lowest total energy of the structure compared to hcp and top sites. The phosphorus atom is then relaxed along with the top 3 gold layers before computing the SCF loop with the following parameters: $E^{\psi}_{cut} = 50$ Ry, $E^{\rho}_{cut} = 300$ Ry, Marzari-Vanderbilt smearing of 0.005 Ry, local-TF (or local-density-dependent Thomas-Fermi screening) mixing mode with $\beta = 0.3$ (for robust convergence) and a $15 \times 15 \times 1$ k-points mesh.
The charge densities, iso-DOS, band structures with and without the phosphorus atom and the projected band structures are computed directly from the SCF results. Band structures are calculated along a 300-k-point $M\Gamma KM$ path in the Brillouin Zone (BZ). All band structure projections are done using the *projwfc.x* code and k-resolved projected DOS calculations along the same 300-k-point path.
All other post-processing calculations - such as DOS, PDOS and LDOS at different heights above the phosphorus atom - are done after an NSCF calculation with a finer mesh of $51 \times 51 \times 1$ k-points and 'tedrahedra' occupations. To compare the LDOS with the experimental dI/dV spectrum, all LDOS have been recomputed after doing an NSCF calculation with cold 'smearing' occupations (Marzari-Vanderbilt)

and a mesh of $27 \times 27 \times 1$ kpoints covering only half of the BZ (in length) around the Γ point. This new mesh is simply made by applying a $\frac{1}{2}$ homothety on the Monkhorst-Pack grid mesh of the full BZ. The LDOS calculations have been performed in boxes at different heights above the phosphorus atom and all are approximately 1Å high and have in-plane lengths of $\frac{1}{2}a_1$ and $\frac{1}{2}a_2$ in $\vec{a}_1$ and $\vec{a}_2$ directions. Additionally, a study of the progressive adsorption of the HexP-monolayer by the Au(111) surface is done using a custom automated AiiDA workflow. This workflow interpolates 19 structures between the relaxed system of P/Au(111), and the relaxed Au(111) surface with the P atom at 5 Å above its relaxed position. For each of these structures the workflow calculates the band structure and the band structure projections. This allows to track bands and orbital contributions in the band structure during the uniform approach of the HexP-monolayer. The corresponding database is not linked but the videos created from this uniform adsorption study are linked in the references [22].

Supporting Information
Supporting Information is available from the Wiley Online Library or from the author.

Acknowledgements
We thank the French National Research Agency (ANR-20-CE09-0023 DEFINE2D, ANR-22-CE09-0022 2DPhostrainE) for financial support.

References

[1] G. Fiori, F. Bonaccorso, G. Iannaccone, T. Palacios, D. Neumaier, A. Seabaugh, S. K. Banerjee, L. Colombo, Nat. Nanotechnol. **2014**, 9, 10 768.

[2] P. Ares, K. S. Novoselov, Nano Mater. Sci. **2022**, 4, 1 3.

[3] A. Carvalho, M. Wang, X. Zhu, A. S. Rodin, H. Su, A. H. Castro Neto, Nat. Rev. Mater. **2016**, 1, 11 1.

[4] Y. Zhou, M. Zhang, Z. Guo, L. Miao, S.-T. Han, Z. Wang, X. Zhang, H. Zhang, Z. Peng, Mater. Horiz. **2017**, 4, 6 997.

[5] W. Zhang, X. Zhang, L. K. Ono, Y. Qi, H. Oughaddou, Small **2024**, 20, 4 2303115.

[6] L. Li, Y. Yu, G. J. Ye, Q. Ge, X. Ou, H. Wu, D. Feng, X. H. Chen, Y. Zhang, Nat. Nanotechnol. **2014**, 9, 5 372.

[7] X. Ling, H. Wang, S. Huang, F. Xia, M. S. Dresselhaus, Proc. Natl. Acad. Sci. **2015**, 112, 15 4523.

[8] F. Xia, H. Wang, J. C. M. Hwang, A. H. C. Neto, L. Yang, Nat. Rev. Phys. **2019**, 1, 5 306.

[9] Y. Wang, S. Sun, J. Zhang, Y. L. Huang, W. Chen, SmartMat **2021**, 2, 3 286.

[10] J. Guan, Z. Zhu, D. Tománek, Phys. Rev. Lett. **2014**, 113, 4 046804.

[11] H. Guo, N. Lu, J. Dai, X. Wu, X. C. Zeng, J. Phys. Chem. C **2014**, 118, 25 14051.

[12] L. Ding, P. Shao, Y. Yin, F. Ding, Adv. Funct. Mater. **2024**, 34, 32 2316612.

[13] Z. Zhu, D. Tománek, Phys. Rev. Lett. **2014**, 112, 17 176802.

[14] J. L. Zhang, S. Zhao, C. Han, Z. Wang, S. Zhong, S. Sun, R. Guo, X. Zhou, C. D. Gu, K. D. Yuan, Z. Li, W. Chen, Nano Lett. **2016**, 16, 8 4903.

[15] C. Gu, S. Zhao, J. L. Zhang, S. Sun, K. Yuan, Z. Hu, C. Han, Z. Ma, L. Wang, F. Huo, W. Huang, Z. Li, W. Chen, ACS Nano **2017**, 11, 5 4943.

[16] J. L. Zhang, S. Zhao, S. Sun, H. Ding, J. Hu, Y. Li, Q. Xu, X. Yu, M. Telychko, J. Su, C. Gu, Y. Zheng, X. Lian, Z. Ma, R. Guo, J. Lu, Z. Sun, J. Zhu, Z. Li, W. Chen, ACS Nano **2020**, 14, 3 3687.

[17] Y. Kaddar, W. Zhang, H. Enriquez, Y. J. Dappe, A. Bendounan, G. Dujardin, O. Mounkachi, A. El kenz, A. Benyoussef, A. Kara, H. Oughaddou, Adv. Funct. Mater. **2023**, 33, 21 2213664.

[18] E. Golias, M. Krivenkov, A. Varykhalov, J. Sánchez-Barriga, O. Rader, Nano lett. **2018**, 18, 11 6672.

[19] J.-P. Xu, J.-Q. Zhang, H. Tian, H. Xu, W. Ho, M. Xie, Phys. Rev. Materials **2017**, 1, 6 061002.

[20] N. Han, N. Gao, J. Zhao, J. Phys. Chem. C **2017**, 121, 33 17893.

[21] J. L. Zhang, S. Zhao, M. Telychko, S. Sun, X. Lian, J. Su, A. Tadich, D. Qi, J. Zhuang, Y. Zheng, Z. Ma, C. Gu, Z. Hu, Y. Du, J. Lu, Z. Li, W. Chen, Nano Lett. **2019**, 19, 8 5340.

[22] I.-E. Michel, Videos of the evolution of the projected band structures of Hexagonal phosphorus monolayer on Au(111) surface during uniform adsorption, **2024**, URL https://doi.org/10.5281/zenodo.11093465.

[23] P. Giannozzi, S. Baroni, N. Bonini, M. Calandra, R. Car, C. Cavazzoni, D. Ceresoli, G. L. Chiarotti, M. Cococcioni, I. Dabo, A. Dal Corso, S. de Gironcoli, S. Fabris, G. Fratesi, R. Gebauer, U. Gerstmann, C. Gougoussis, A. Kokalj, M. Lazzeri, L. Martin-Samos, N. Marzari, F. Mauri, R. Mazzarello, S. Paolini, A. Pasquarello, L. Paulatto, C. Sbraccia, S. Scandolo, G. Sclauzero, A. P. Seitsonen, A. Smogunov, P. Umari, R. M. Wentzcovitch, J. Phys.: Condens. Matter **2009**, 21, 39 395502.

[24] P. Giannozzi, O. Andreussi, T. Brumme, O. Bunau, M. B. Nardelli, M. Calandra, R. Car, C. Cavazzoni, D. Ceresoli, M. Cococcioni, N. Colonna, I. Carnimeo, A. D. Corso, S. de Gironcoli, P. Delugas, R. A. D. Jr, A. Ferretti, A. Floris, G. Fratesi, G. Fugallo, R. Gebauer, U. Gerstmann, F. Giustino, T. Gorni, J. Jia, M. Kawamura, H.-Y. Ko, A. Kokalj, E. Küçükbenli, M. Lazzeri, M. Marsili, N. Marzari, F. Mauri, N. L. Nguyen, H.-V. Nguyen, A. O. de-la Roza, L. Paulatto, S. Poncé, D. Rocca, R. Sabatini, B. Santra, M. Schlipf, A. P. Seitsonen, A. Smogunov, I. Timrov, T. Thonhauser, P. Umari, N. Vast, X. Wu, S. Baroni, J. Phys.: Condens. Matter **2017**, 29, 46 465901.

[25] Aiida 2.5.1 documentation, URL https://aiida.readthedocs.io/projects/aiida-core/en/stable/.

[26] S. P. Huber, S. Zoupanos, M. Uhrin, L. Talirz, L. Kahle, R. Häuselmann, D. Gresch, T. Müller, A. V. Yakutovich, C. W. Andersen, F. F. Ramirez, C. S. Adorf, F. Gargiulo, S. Kumbhar, E. Passaro, C. Johnston, A. Merkys, A. Cepellotti, N. Mounet, N. Marzari, B. Kozinsky, G. Pizzi, Sci. Data **2020**, 7 300.

[27] M. Uhrin, S. P. Huber, J. Yu, N. Marzari, G. Pizzi, Comp. Mater. Sci. **2021**, 187 110086.

[28] I.-E. Michel, AiiDA archive of the study of electronic properties of HexP-Monolayer on Au(111) using Quantum ESPRESSO framework, **2024**, URL https://doi.org/10.5281/zenodo.11075446.

[29] P. A. Schultz, Phys. Rev. B **2021**, 103, 19 195426.

[30] J. P. Perdew, A. Ruzsinszky, G. I. Csonka, O. A. Vydrov, G. E. Scuseria, L. A. Constantin, X. Zhou, K. Burke, Phys. Rev. Lett. **2008**, 100 136406.

Table of Contents

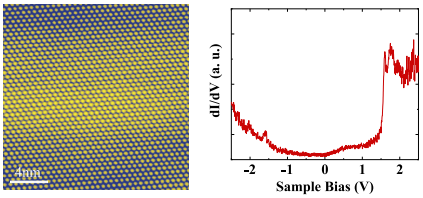

Hexagonal phosphorus nanostructures and monolayer have been grown on Au(111). The progressive formation of unoccupied electronic bands involving substrate mediated coupling between phosphorus atoms have been observed and explained by combining scanning tunneling microscopy and *ab initio* calculations.